Ultrasonic study of terbium in a magnetic field*

S. Maekawa,† R. A. Treder, M. Tachiki,‡ M. C. Lee,§ and M. Levy
University of Wisconsin-Milwaukee, Milwaukee, Wisconsin 53201
(Received 16 July 1975)

A model is presented which describes longitudinal ultrasonic propagation characteristics in magnetic materials. The model specifically incorporates magnetoelastic and exchange interactions when an external magnetic field is applied. Spin fluctuations and spin polarization are seen to play a dominant role, and particular attention is focused on the effect of critical fluctuations near the magnetic-phase-transition temperatures. The model is applied to single-crystal terbium. Longitudinal ultrasonic attenuation data are presented under conditions of constant temperature and constant magnetic field. The constant-temperature data reveal a very large attenuation enhancement by a magnetic field in the paramagnetic region. The constant-field data show anomalous attenuation maxima even when the applied field is sufficient to quench the spin-spiral state; a magnetic phase diagram for terbium is deduced from the constant-field data. A quantitative comparison between the experimental results and theory is presented for the constant-temperature data, and a qualitative comparison between experimental results and theory is presented for the constant-field data. Good agreement is achieved.

I. INTRODUCTION

Terbium has very strong magnetoelastic coupling, indicating that changes in its spin ordering (due to temperature changes or application of magnetic field) will significantly affect its ultrasonic-attenuation and velocity characteristics. Experimental studies of the ultrasonic velocity and zero-field ultrasonic attenuation have already been reported.[1-3] We shall report on the ultrasonic attenuation in terbium for nonzero applied magnetic field.

Our experimental measurements show that for temperatures above the Néel temperature, the constant-temperature attenuation in terbium first increases with the magnetic field, then reaches a maximum and decreases as the magnetic field increases. Near the Néel temperature the application of a magnetic field increases the ultrasonic attenuation by an order of magnitude. We have found, in addition, a very complicated temperature dependence of the attenuation, depending strongly on the magnetic field applied: A double-peak structure occurs for low magnetic fields and the two peaks appear to correspond to the Néel and Curie transitions; at the intermediate field strengths only one peak is discernible; at higher fields, the temperature dependence again exhibits a double-peak structure. Luthi *et al.*[4] have reported anomalous divergent behavior of the velocity variation with temperature near T_N in Tb under a magnetic field.

A recent theory developed by two of the present authors (M.T. and S.M.), and applied in particular to the experimental results on MnP found by Komatsubara *et al.*,[5,6] is modified in this paper to explain these experimental results; the modification consists of the explicit inclusion of the magnetostriction as well as the magnetic field in the expression of the spin fluctuations. This model considers the atomic lattice and spin system as coupled via the exchange and single-ion magnetoelastic interactions: The theory regards the coupled lattice and spins as the unperturbed system; the time-dependent modulation of the lattice-spin coupling which accompanies the impressed ultrasonic wave is regarded as a perturbation. Phonon absorption by the spin system produces the sound attenuation.

Of particular interest in this paper is the critical attenuation of sound near a magnetic phase transition, such as near the Néel temperature or Curie temperature. In the vicinity of these phase transitions the fluctuating spins have components which become relatively strongly correlated, the correlation strength being governed by the proximity to the transition temperature. This correlation of spin components essentially increases the effectiveness of the spin-lattice coupling, giving a corresponding increase in the ultrasonic attenuation.

Our experimental results appear to be explained by the effect of the magnetic field on the spin polarization and fluctuations of the spins which we have incorporated into our model. This model starts with a random-phase approximation in which the attenuation coefficient is expressed as a sum of two terms: A cross term of the static spin polarization with the two-spin correlation function parallel to the field, and a sum of products of four-spin correlation functions which are later decoupled into two-spin correlation functions. In the magnetic field the maximum of the two-spin correlation function occurs at different tempera-

tures for different directions, and each component of the correlation function contributes to the attenuation in a different way. This has allowed us to interpret the double-peak structure observed in the high-field region. The constant-temperature attenuation behavior and the velocity variation for temperatures above T_N can also be explained on the basis of this model. In this way we have reduced the information to a magnetic phase diagram for terbium which gives an overview of the magnetic field effects we have found for this element.

II. THEORY

Terbium metal has a spin-spiral structure for only a narrow temperature range between 227 and 221 °K. Its spin-spiral axis is along the c axis and the spins are in the c plane of the hexagonal-close-packed (hcp) crystal structure. The spin-spiral turn angle is around 18°, which is small compared to that of the other rare-earth metals. At 220 °K a first-order phase transition occurs and the spins align in the c plane ferromagnetically. There is appreciable lattice distortion at this temperature ($\delta l/l \approx 10^{-2}-10^{-3}$). According to Cooper[7,9] the transition occurs because there is competition between the exchange interaction for the undistorted hcp lattice favoring a spin-spiral arrangement on the one hand, and the magnetostriction favoring a ferromagnetic arrangement on the other hand. The reason that the transition occurs is that the temperature dependences of these different contributions to the free energy differ. The magnetostrictive energy is larger at low temperatures than the difference between the spin-spiral and ferromagnetic exchange energies. However, it falls more sharply than this difference with increasing temperature, so that at high temperatures exchange effects for the undistorted lattice dominate. A magnetic field in the c plane narrows the temperature span of the spin-spiral phase. At a certain value of the field, the spin-spiral phase disappears and above this field the spin system is uniform at any temperature.

We should emphasize the following two points: First, the energies between the ferromagnetic and spin-spiral states are very close. Second, the magnetoelastic interaction has an effect on the ferromagnetic phase transition which is comparable in magnitude to that of the exchange interaction.

The Hamiltonian for Tb is expressed as

$$\mathcal{H}=\mathcal{H}_m+\mathcal{H}_{an}+\mathcal{H}_e+\mathcal{H}_{me}+\mathcal{H}_{ph}+\mathcal{H}_{s-ph}. \tag{2.1}$$

$\mathcal{H}_m$ denotes the exchange interaction and the Zeeman term:

$$\mathcal{H}_m=-\sum_{i,j} J_{ij}\,\vec{\mathbf{S}}_i\cdot\vec{\mathbf{S}}_j+g\mu_B H\sum_i S_{iz}\ , \tag{2.2}$$

where $\vec{\mathbf{S}}_i$ is the total angular momentum at the ith site. Hereafter, the total angular momentum is called spin. g is the Landé g factor which is $\frac{3}{2}$ for Tb. The case we consider is that of a magnetic field applied in the c plane. The x axis is taken parallel to the magnetic field, the y axis perpendicular to the field in the c plane, and the z axis parallel to the c axis.

For the hcp lattice of Tb, there exist four magnetic anisotropy constants.[10] Of these anisotropy constants, the second-order anisotropy constant K_2 is the largest.[11-16] The fourth-order anisotropy constant K_4 is one order of magnitude smaller than K_2 at 0 °K.[15] From torque measurements on a dilute solution of Tb in Gd, it has been shown that the sixth-order uniaxial anisotropy constant K_6 is about 30% of K_4.[17] The sixfold basal-plane anisotropy constant K_6^6 is two orders of magnitude smaller than K_2.[11,18] The effect of K_6^6 on the spin-spiral to ferromagnetic transition is negligible compared with the magnetoelastic effect.[8] Therefore, we only retain the anisotropy energy which corresponds to K_2 and write the spin Hamiltonian as

$$\mathcal{H}_{an}=D\sum_i\left[S_{iz}^2-\tfrac{1}{3}S(S+1)\right],\quad D=\frac{3K_2}{S(2S-1)}>0. \tag{2.3}$$

$\mathcal{H}_e$ denotes the elastic energy for the system. The complete expression for the hexagonal lattice has been given by Callen and Callen.[19] According to them, $\mathcal{H}_e$ has the following form:

$$\mathcal{H}_e=\tfrac{1}{2}c_{11}^{\alpha}(\epsilon^{\alpha,1})^2+c_{12}^{\alpha}\epsilon^{\alpha,1}\epsilon^{\alpha,2}+\tfrac{1}{2}c_{22}^{\alpha}(\epsilon^{\alpha,2})^2 +\tfrac{1}{2}c^{\gamma}\left[(\epsilon_1^{\gamma})^2+(\epsilon_2^{\gamma})^2\right]+\tfrac{1}{2}c^{\epsilon}\left[(\epsilon_1^{\epsilon})^2+(\epsilon_2^{\epsilon})^2\right], \tag{2.4}$$

where

$$\begin{aligned}&\epsilon^{\alpha,1}=\epsilon_{xx}+\epsilon_{yy}+\epsilon_{zz}\ ,\\ &\epsilon^{\alpha,2}=(\tfrac{1}{2}\sqrt{3})(\epsilon^{zz}-\tfrac{1}{3}\epsilon^{\alpha,1}),\\ &\epsilon_1^{\gamma}=\tfrac{1}{2}(\epsilon_{xx}-\epsilon_{yy}),\ \epsilon_2^{\gamma}=\epsilon_{xy}\ ,\\ &\epsilon_1^{\epsilon}=\epsilon_{zy},\ \epsilon_2^{\epsilon}=\epsilon_{xz}.\end{aligned} \tag{2.5}$$

The symmetry elastic constants are related to the conventional Cartesian elastic constants by

$$\begin{aligned}&c_{11}^{\alpha}=\tfrac{1}{9}(2c_{11}+2c_{12}+4c_{13}+c_{33}),\\ &c_{12}^{\alpha}=(2/3\sqrt{3})(-c_{11}-c_{12}+c_{13}+c_{33}),\\ &c_{22}^{\alpha}=\tfrac{2}{3}c_{11}+\tfrac{2}{3}c_{12}-\tfrac{8}{3}c_{13}+\tfrac{4}{3}c_{33},\\ &c^{\gamma}=2(c_{11}-c_{12}),\ c^{\epsilon}=4c_{44}.\end{aligned} \tag{2.6}$$

All the elastic constants of Tb have been mea-

sured at room temperature by Jenson.[2] His results show that $c_{12}^{\alpha}=0.11\times10^{11}$ dyn/cm^3, which is about two orders of magnitude smaller than other elastic constants. Therefore we assume that c_{12}^{α} in Tb vanishes and, thus, the $(\alpha,1)$ and $(\alpha,2)$ strains are not coupled.

The magnetoelastic Hamiltonian $\mathcal{H}_{\rm me}$ for a hcp crystal has been given by Callen and Callen[19]:

$$\mathcal{H}_{\rm me}=-\sum_{ij}\left[\left(\tilde{D}_{11}^{\alpha}(ij)-\frac{\sqrt{3}}{6}\tilde{D}_{12}^{\alpha}(ij)\right)\epsilon^{\alpha,1}+\left(\tilde{D}_{21}^{\alpha}(ij)-\frac{\sqrt{3}}{6}\tilde{D}_{22}^{\alpha}(ij)\right)\epsilon^{\alpha,2}\right]\vec{S}_i\cdot\vec{S}_j$$
$$-\sum_{ij}\left(\frac{\sqrt{3}}{2}\tilde{D}_{12}^{\alpha}(ij)\epsilon^{\alpha,1}+\frac{\sqrt{3}}{2}\tilde{D}_{22}^{\alpha}(ij)\epsilon^{\alpha,2}\right)S_{iz}S_{jz}-\sum_{i}(\tilde{B}_{12}^{\alpha}\epsilon^{\alpha,1}+\tilde{B}_{22}^{\alpha}\epsilon^{\alpha,2})\,(\sqrt{3}/2)\,[S_{iz}^2-\tfrac{1}{3}S(S+1)]$$
$$-\sum_{i}\tilde{B}^{\gamma}[\epsilon_1^{\gamma\frac{1}{2}}(S_{ix}^2-S_{iy}^2)+\epsilon_2^{\gamma\frac{1}{2}}(S_{ix}S_{iy}+S_{iy}S_{ix})]-\sum_{i}\tilde{B}^{\epsilon}[\epsilon_1^{\epsilon\frac{1}{2}}(S_{iy}S_{iz}+S_{iz}S_{iy})+\epsilon_2^{\epsilon\frac{1}{2}}(S_{ix}S_{iz}+S_{iz}S_{ix})]\,. \tag{2.7}$$

In the above Hamiltonian, the two-ion–type terms for the γ and ϵ strains were neglected because the single-ion theory provides a good fit to the experimental data on the temperature dependence of these strains in Tb[20] and Dy.[21] $\mathcal{H}_{\rm ph}$ represents the Hamiltonian for the noninteracting longitudinal acoustic phonons:

$$\mathcal{H}_{\rm ph}=\sum_{\vec{k}}\hbar\omega_{\vec{k}}^{0}b_{\vec{k}}^{\dagger}b_{\vec{k}}\,, \tag{2.8}$$

where $\omega_{\vec{k}}^{0}$ is its frequency, and the operators $b_{\vec{k}}$ and $b_{\vec{k}}^{\dagger}$ are annihilation- and creation-boson operators, respectively. The longitudinal acoustic wave along the c axis couples to the spin system through the strain modulation of the exchange and magnetostrictive interactions. When the strain ϵ_{zz} in $\epsilon^{\alpha,1}$ and $\epsilon^{\alpha,2}$ is expressed by the derivative of the lattice displacement and the displacement is expressed by the phonon operators, this interaction Hamiltonian in the long-wavelength limit is obtained as

$$\mathcal{H}_{s\text{-ph}}=\sum_{\vec{k}}(\hbar/2\rho V\omega_{\vec{k}}^{0})^{1/2}(b_{\vec{k}}+b_{-\vec{k}}^{\dagger})(U_{\vec{k},1}+U_{\vec{k},2}), \tag{2.9}$$

$$U_{\vec{k},1}=-\sum_{ij}\sum_{\mu}g_{ij}^{\mu*}(\vec{k})e^{i\vec{k}\cdot\vec{R}_i}S_{i\mu}S_{j\mu}\,, \tag{2.10}$$

$$U_{\vec{k},2}=-\sum_{i}h^{*}(\vec{k})e^{i\vec{k}\cdot\vec{R}_i}[S_{iz}^2-\tfrac{1}{3}S(S+1)], \tag{2.11}$$

$$g_{ij}^{\mu}(\vec{k})=i(\vec{k}\cdot\vec{e}_k)\left[\tilde{D}_{11}^{\alpha}(ij)-\frac{\sqrt{3}}{6}\tilde{D}_{12}^{\alpha}(ij)+\frac{1}{\sqrt{3}}\tilde{D}_{21}^{\alpha}(ij)-\tfrac{1}{6}\tilde{D}_{22}^{\alpha}(ij)\right]\quad\text{for }\mu=x\text{ and }y, \tag{2.12}$$

$$g_{ij}^{z}(\vec{k})=i(\vec{k}\cdot\vec{e}_k)\left[\tilde{D}_{11}^{\alpha}(ij)+\frac{1}{\sqrt{3}}\tilde{D}_{12}^{\alpha}(ij)+\frac{1}{\sqrt{3}}\tilde{D}_{21}^{\alpha}(ij)+\tfrac{1}{3}\tilde{D}_{22}^{\alpha}(ij)\right],$$

$$h(\vec{k})=i(\vec{k}\cdot\vec{e}_k)\left(\frac{\sqrt{3}}{2}\tilde{B}_{12}^{\alpha}+\tfrac{1}{2}\tilde{B}_{22}^{\alpha}\right), \tag{2.13}$$

where ρ is the density of the crystal, V is the volume, and $e_{\vec{k}}$ is the polarization vector of the phonons with the wave number k which is parallel to the c axis in the z direction. The variation of T_N has been observed to be linear with pressure in Tb and Dy.[22,23] Therefore, the higher-order effects with respect to strains and phonon amplitudes were not included in Eqs. (2.7) and (2.9).

We calculate the free energy from the Hamiltonian (2.1) using the mean-field approximation and obtain $\epsilon_i^{\Gamma,j}$ from the relation $\partial F/\partial\epsilon_i^{\Gamma,j}=0$ as

$$\epsilon^{\alpha,1}=\frac{1}{c_{22}^{\alpha}}\left(\tilde{D}_{11}^{\alpha}(0)-\frac{\sqrt{3}}{6}\tilde{D}_{12}^{\alpha}(0)\right)\left(\frac{A_1}{A_0}\right)^2$$
$$+\frac{\sqrt{3}}{2c_{11}^{\alpha}}\tilde{B}_{12}^{\alpha}[\tfrac{1}{6}S(S+1)-A_2/2A_0], \tag{2.14}$$

$$\epsilon^{\alpha,2}=\frac{1}{c_{22}^{\alpha}}\left(\tilde{D}_{21}^{\alpha}(0)-\frac{\sqrt{3}}{6}\tilde{D}_{22}^{\alpha}(0)\right)\left(\frac{A_1}{A_0}\right)^2$$
$$+\frac{\sqrt{3}}{2c_{22}^{\alpha}}\tilde{B}_{22}^{\alpha}[\tfrac{1}{6}S(S+1)-A_2/2A_0], \tag{2.15}$$

$$\epsilon_1^\gamma = \frac{\tilde{B}^\gamma}{4c^\gamma}[S(S+1) - 3(A_2/A_0)], \tag{2.16}$$

where $\tilde{D}^\alpha_{mn}(0)$ is the component with $q=0$ of $\tilde{D}^\alpha_{mn}(\vec{q})$ defined by

$$\tilde{D}^\alpha_{mn}(\vec{q}) = \sum_{ij} \tilde{D}^\alpha_{mn}(ij) e^{i\vec{q}\cdot(\vec{R}_j - \vec{R}_i)}. \tag{2.17}$$

The other strains are zero. In Eqs. (2.14)–(2.16), A_n is defined by $A_n = \mathrm{Tr}(S_z)^n \exp(-\beta \mathcal{H}_{\mathrm{mf}})$ with the mean-field Hamiltonian $\mathcal{H}_{\mathrm{mf}}$. By following the mean-field theory in the usual way, the magnetization in the paramagnetic and ferromagnetic phases is calculated from the self-consistent equation

$$\sigma_x = \langle S_x \rangle = [A_1/A_0 - \tfrac{1}{2}\beta(-\tilde{D} + \tfrac{3}{2}\tilde{\beta}^\gamma \epsilon_1^\gamma)(A_3/A_0 - A_1A_2/A_0^2)], \tag{2.18}$$

$$\tilde{D} = D - \frac{\sqrt{3}}{2}(\tilde{B}^\alpha_{12}\epsilon^{\alpha,1} + \tilde{B}^\alpha_{22}\epsilon^{\alpha,2}). \tag{2.19}$$

When a staggered magnetic field H^μ_q is applied along the μ axis, the mean-field Hamiltonian for the ith spin is expressed as

$$\mathcal{H}_{\mathrm{mf}}(i) = (-2\tilde{J}^z_0\sigma_x + g\mu_B H)S_{ix} + \tilde{D}S^2_{iz} - \tfrac{1}{2}\tilde{B}^\gamma\epsilon_1^\gamma(S^2_{ix} - S^2_{iy}) + (-2\tilde{J}^\mu_q\langle S^\mu_{\vec{q}}\rangle/\sqrt{N} + g\mu_B H^\mu_{\vec{q}})e^{-i\vec{q}\cdot\vec{R}_i}S_{i\mu}, \tag{2.20}$$

where

$$\tilde{J}^\mu_{\vec{q}} = J_{\vec{q}} + \left(\tilde{D}^\alpha_{11}(\vec{q}) - \frac{\sqrt{3}}{6}\tilde{D}^\alpha_{12}(\vec{q})\epsilon^{\alpha,1} + (\tilde{D}^\alpha_{21}(\vec{q}) - \frac{\sqrt{3}}{6}\tilde{D}^\alpha_{22}(\vec{q}))\epsilon^{\alpha,2}\right) + \left(\frac{\sqrt{3}}{2}\tilde{D}^\alpha_{12}(\vec{q})\epsilon^{\alpha,1} + \frac{\sqrt{3}}{2}\tilde{D}^\alpha_{22}(\vec{q})\epsilon^{\alpha,2}\right)\delta_{\mu z}, \tag{2.21}$$

$$J_{\vec{q}} = \sum_{i-j} J_{ij} e^{i\vec{q}\cdot(\vec{R}_i - \vec{R}_j)}, \tag{2.22}$$

$$S^\mu_{\vec{q}} = \frac{1}{\sqrt{N}}\sum_i (S_{i\mu} - \sigma_x\delta_{\mu x})e^{i\vec{q}\cdot\vec{R}_i}. \tag{2.23}$$

In Eq. (2.20), we divided the component S^x_0 into the static spin polarization $S^x_0 = \sqrt{N}\sigma_x$ and the deviation $S^{x'}_0$ from it:

$$S^x_0 = \langle S^x_0\rangle + S^{x'}_0. \tag{2.24}$$

Therefore, $\langle S^\mu_{\vec{q}}\rangle$ with $\vec{q}=0$ and $\mu = x$ in Eq. (2.20) should read $\langle S^{x'}_0\rangle$. We obtain the staggered spin polarization by solving the self-consistent equation

$$\langle S^\mu_{\vec{q}}\rangle = \frac{1}{\sqrt{N}}\sum_i \frac{e^{i\vec{q}\cdot\vec{R}_i}\,\mathrm{Tr}(S_{i\mu} - \sigma_x\delta_{\mu x})\exp[-\beta\mathcal{H}_{\mathrm{mf}}(i)]}{\mathrm{Tr}\exp[-\beta\mathcal{H}_{\mathrm{mf}}(i)]}. \tag{2.25}$$

The diagonal element of the staggered susceptibility defined by

$$\chi^\mu_{\vec{q}} = -\lim_{H^\mu_{\vec{q}}\to 0} q\mu_B\langle S^\mu_{\vec{q}}\rangle/\sqrt{N}H^\mu_{\vec{q}} \tag{2.26}$$

is calculated as

$$\chi^\mu_{\vec{q}} = g^2\mu_B^2 G_\mu/(1 - 2\tilde{J}^\mu_{\vec{q}}G_\mu). \tag{2.27}$$

The definition of G_μ is given in the Appendix. In the above calculation we used the frozen-lattice model.[8]

The large anisotropy energy strongly suppresses the spin fluctuation along the c axis and $\chi^z_{\vec{q}}$ becomes very small. The magnetostrictive interaction suppresses the spin fluctuation perpendicular to the magnetic field in the basal plane and decreases $\chi^y_{\vec{q}}$. We indicate by $\vec{Q}$ the wave number at which $\tilde{J}^y_{\vec{q}}$ has its maximum. Then, $\chi^y_{\vec{Q}}$ diverges at a certain temperature under a magnetic field, and a sinusoidal spin order with wave number Q and with an infinitesimal amplitude appears along the y axis at this temperature. We call this temperature the Néel temperature. The Néel temperature decreases with increasing magnetic field. Above a critical magnetic field H_c, the constraints on the spin motion reduce the fluctuations such that the divergence in $\chi^y_{\vec{Q}}$ disappears, resulting in the disappearance of T_N. However, even under magnetic fields above H_c, $\chi^y_{\vec{q}}$ has a maximum when the temperature changes. This maximum leads to an anomalous peak of the attenuation coefficient of longitudinal sound waves. $\chi^z_{\vec{q}}$ does not diverge at any temperature under a finite magnetic field.

III. ULTRASONIC-ATTENUATION COEFFICIENT

Previous theoretical studies of ultrasonic attenuation due to the spin-phonon interaction[24] were preceded by the more general theories of irreversible processes by Kubo[25] and Mori[26] applied to magnetic systems. Tachiki and Maekawa[5] explicitly calculated the ultrasonic-attenuation coefficient for a spin system to which a magnetic field has been applied. The procedure used by Tachiki and Maekawa will be followed here in the calculation of the attenuation coefficient for a longitudinal sound wave in Tb.

The ultrasonic-attenuation coefficient is expressed as a function of the time correlation of the random force acting on the phonon as

$$\alpha_{\vec{k}} = \mathrm{Re}\int_0^\infty dt\langle f_{\vec{k}}(t),\ f^*_{\vec{k}}(0)\rangle e^{-i\omega_{\vec{k}}t}/v_l\,(b_{\vec{k}}, b^\dagger_{\vec{k}}), \tag{3.1}$$

with the relaxation function defined by

$$(A, B) = \int_0^\beta d\lambda \langle e^{\lambda \mathcal{H}} A e^{-\lambda \mathcal{H}} B\rangle - \beta\langle A\rangle\langle B\rangle .$$

In Eq. (3.1), v_l is the speed of the longitudinal sound wave and the random force is defined by

$$f_{\vec{k}} = \dot{b}_{\vec{k}} + i\omega_{\vec{k}} b_{\vec{k}}. \tag{3.2}$$

If the relation

$$\omega_{\vec{k}} = i(\dot{b}_{\vec{k}}, b_{\vec{k}}^\dagger)/(b_{\vec{k}}, b_{\vec{k}}^\dagger) = \langle [b_{\vec{k}}, b_{\vec{k}}^\dagger]\rangle /\hbar(b_{\vec{k}}, b_{\vec{k}}^\dagger) = 1/\hbar(b_{\vec{k}}, b_{\vec{k}}^\dagger), \tag{3.3}$$

is used, $(b_{\vec{k}}, b_{\vec{k}}^\dagger)$ is related to the phonon frequency $\omega_{\vec{k}}$. The frequency is changed by the spin-phonon interaction. However, since this change is very small, $\omega_{\vec{k}}$ and v_l in Eq. (3.1) are replaced by those of noninteracting phonons. The random force is obtained from Eq. (3.2) as

$$f_{\vec{k}} = -i(2\rho V\hbar\omega_{\vec{k}}^0)^{-1/2}(U_{-\vec{k},1} + U_{-\vec{k},2}), \tag{3.4}$$

where $U_{-\vec{k},1}$ and $U_{-\vec{k},2}$ were given in Eqs. (2.10) and (2.11). By using Eqs. (2.23), (3.3), and (3.4), the attenuation coefficient (3.1) is calculated as

$$\alpha_{\vec{k}} = (2\rho V v_l)^{-1}\mathrm{Re}\sum_{\vec{q}}\sum_{\vec{q}'}\int_0^\infty dt\, e^{-i\omega_{\vec{k}}t}\left(\left[\sum_\alpha g_{\vec{q}}^{\alpha *}(\vec{k}) S_{\vec{q}}^\alpha(t) S_{-\vec{q}-\vec{k}}^\alpha(t) + h^*(\vec{k}) S_{\vec{q}}^z(t) S_{-\vec{q}-\vec{k}}^z(t)\right],\right.$$
$$\left.\times\left[\sum_\alpha g_{\vec{q}'}^{\alpha'}(\vec{k}) S_{-\vec{q}'}^{\alpha'}(0) S_{\vec{q}'+\vec{k}}^{\alpha'}(0) + h(\vec{k}) S_{-\vec{q}'}^z(0) S_{-\vec{q}'+\vec{k}}^z(0)\right]\right), \tag{3.5}$$

$$g_{\vec{q}}^\alpha(\vec{k}) = \sum_{ij} e^{i\vec{q}\cdot\vec{R}_{ji}}\, i(\vec{k}\cdot\vec{e}_{\vec{k}}) g_{ij}^\alpha(\vec{k}). \tag{3.6}$$

The magnetic field induces a uniform spin polarization in the x direction and spins fluctuate around it. If Eq. (2.24) is used, the attenuation coefficient is rewritten as

$$\alpha_{\vec{k}} = (2\rho V v_l)^{-1}\mathrm{Re}\left\{4g_0^{x*}(\vec{k}) g_0^x(\vec{k})\langle S_0^x\rangle^2 \int_0^\infty (S_{-\vec{k}}^x(t), S_{\vec{k}}^x(0))\, e^{-i\omega_{\vec{k}}t}\, dt\right.$$
$$+\sum_{\vec{q}}\sum_{\vec{q}'}\int_0^\infty dt\, e^{-i\omega_{\vec{k}}t}\left(\left[\sum_\alpha g_{\vec{q}}^{\alpha *}(\vec{k}) S_{\vec{q}}^\alpha(t) S_{-\vec{q}-\vec{k}}^\alpha(t) + h^*(\vec{k}) S_{\vec{q}}^z(t) S_{-\vec{q}-\vec{k}}^z(t)\right],\right.$$
$$\left.\left.\times\left[\sum_{\alpha'} g_{\vec{q}'}^{\alpha'}(\vec{k}) S_{-\vec{q}'}^{\alpha'}(0) S_{\vec{q}'+\vec{k}}^{\alpha'}(0) + h(\vec{k}) S_{-\vec{q}'}^z(0) S_{\vec{q}'+\vec{k}}^z(0)\right]\right)\right\}, \tag{3.7}$$

where $S_{\vec{k}}^\alpha$ with $\vec{k}=0$ and $\alpha = x$ in the last term reads $S_0^{x'}$. For the calculation of the second term in the large parentheses of Eq. (3.7), we approximate the four-spin relaxation function by products of the two-spin relaxation functions with the use of the decoupling approximation

$$(ab, cd) \sim \beta^{-1}[(a, b)(c, d) + (a, c)(b, d) + (a, d)(b, c) - \beta\langle ab\rangle\langle cd\rangle].$$

In the spin systems of metals the exchange interaction is of long range; hence, this decoupling approximation may work well, except very near the transition temperature where the correlation length of the spin pair correlation function becomes much longer than the force range of the exchange interaction.

The next step to be done is to calculate the two-spin relaxation function in a magnetic field. The time dependence of the spin motion has the form $S_{\vec{q}}^\alpha(t) = S_{\vec{q}}^\alpha \exp(i\omega_{\vec{q}}^\alpha t - \Gamma_{\vec{q}}^\alpha t)$, where $\omega_{\vec{q}}^\alpha$ and $\Gamma_{\vec{q}}^\alpha$ are the frequency and damping constants of the spin $S_{\vec{q}}^\alpha$. However, it has been shown[4] that the attenuation coefficient is almost independent of $\omega_{\vec{q}}^\alpha$. Therefore, neglecting $\omega_{\vec{q}}^\alpha$, we take

$$(S_{\vec{q}}^\alpha(t),\ S_{-\vec{q}}^{\alpha'}(0)) = (S_{\vec{q}}^\alpha, S_{-\vec{q}}^\alpha)\exp(-\Gamma_{\vec{q}}^\alpha t)\delta_{\alpha\alpha'}, \tag{3.8}$$

$$(S_{\vec{q}}^\alpha, S_{-\vec{q}}^\alpha) = (g\mu_B)^{-2}\chi_{\vec{q}}^\alpha. \tag{3.9}$$

In the case that the energy of the spin system is dissipated by conduction electrons through the so-called s-f interaction, it has been shown in Ref. 4 that $\Gamma_{\vec{q}}^\alpha$ may be expressed as

$$\Gamma_{\vec{q}}^\alpha = \beta(g\mu_B)^2 B/\chi_{\vec{q}}^\alpha, \tag{3.10}$$

where B is a constant independent of temperature. We assume Eq. (3.10) for the damping constant of the spins in Tb. According to the neutron-inelastic-scattering experiment on Tb by Dietrich and Als-Nielsen,[27] $\Gamma_{\vec{Q}}^x$ is proportional to $(T - T_N)^{0.92}$ and $\chi_{\vec{Q}}^x$ is proportional to $(T - T_N)^{-1.20}$. In what follows, the assumptions $\Gamma_{\vec{Q}}^x \sim (T - T_N)^{1.0}$ and $\chi_{\vec{Q}}^x \sim (T - T_N)^{1.0}$ appear to be reasonable approximations in view

of the above experimental results.

Using Eqs. (3.8)–(3.10) we obtain $\alpha_{\vec{k}}$ in the case of $\Gamma_{\vec{q}}^{q} \gg \omega_{\vec{k}}$ as

$$\alpha_{\vec{k}} = \frac{1}{2\rho V v_t (g\mu_B)^6 B\beta^2}\Big(4\beta|g_0^x(\vec{k})|^2(g\mu_B\langle S_0^x\rangle)^2(\chi_{\vec{k}}^x)^2 + \sum_{\vec{q}}|g_{\vec{q}}^x(\vec{k})|^2(\chi_{\vec{q}}^x)^3 + \sum_{\vec{q}}|g_{\vec{q}}^y(\vec{k})|^2(\chi_{\vec{q}}^x)^3 + \sum_{\vec{q}}|g_{\vec{q}}^z(\vec{k})+h(\vec{k})|^2\chi_{\vec{q}}^{z3}\Big). \tag{3.11}$$

The exchange constant (2.21) includes the strain-dependent parts which are temperature and field dependent. However, we neglect these parts which are very small compared with the usual exchange constant. The value of $\vec{Q}$ for Tb is about $0.1(2\pi/c_0)$, where c_0 is the lattice constant along the c axis and this value of $\vec{Q}$ is small. Therefore, we expand $J_{\vec{q}}$ for small $\vec{q}$ from Eq. (2.21) and obtain

$$2J_{\vec{q}} = 2J_0 + D_{\parallel}q_z^2 - Aq_z^4 - D_{\perp}(q_y^2+q_x^2), \tag{3.12}$$

where J_0, $D_{\parallel}$, $D_{\perp}$, and A are positive constants. The condition that $J_{\vec{q}}$ should have a maximum at the wave number $\vec{Q}$ gives a relation between $D_{\parallel}$ and A

$$D_{\parallel}/2A = Q^2. \tag{3.13}$$

Inserting the value of J_q from Eq. (3.12) into Eq. (2.27) and then inserting the resulting value of $\chi_{\vec{q}}^{\mu}$ into Eq. (3.11) and summing $\vec{q}$ in Eq. (3.11) over the Brillouin zone, we have

$$\alpha_{\vec{k}} = k_BTF_{\vec{k}}\Big[4\Big(\frac{\sigma_x G_x}{1-2J_0G_x}\Big)^2 + \frac{k_BTv_0}{8\pi D_{\perp}}\Big(\frac{A}{\omega_x}\Big)^{3/2}\frac{\frac{3}{2}\omega_x + D_{\parallel}\omega_x^{1/2} - D_{\parallel}^2}{(\omega_x - D_{\parallel}^2)(\omega_x^{1/2}-D_{\parallel})^{1/2}} + \frac{k_BTv_0}{8\pi D_{\perp}}\Big(\frac{A}{\omega_y}\Big)^{3/2}\frac{\frac{3}{2}\omega_y + D_{\parallel}\omega_y^{1/2} - D_{\parallel}^2}{(\omega_y - D_{\parallel}^2)(\omega_y^{1/2}-D_{\parallel})^{1/2}}$$
$$+ \frac{k_BTv_0}{8\pi D_{\perp}}\frac{|g_0^z(\vec{k})+h(\vec{k})|^2}{|g_0^x(\vec{k})|^2}\Big(\frac{A}{\omega_z}\Big)^{3/2}\frac{\frac{3}{2}\omega_z + D_{\parallel}\omega_z^{1/2} - D_{\parallel}^2}{(\omega_z - D_{\parallel}^2)(\omega_z^{1/2}-D_{\parallel})^{1/2}}\Big], \tag{3.14}$$

$$\omega_{\alpha} = 4A(1-2J_0G_{\alpha})/G_{\alpha}, \tag{3.15}$$

$$F_{\vec{k}} = N|g_0^x(\vec{k})|^2/2\rho V v_t B, \tag{3.16}$$

where v_0 is the volume per spin. In the paramagnetic phase and in the absence of a magnetic field, Eq. (3.14) reduces to the usual mean-field-theory result which gives $\alpha_{\vec{k}}$ proportional to $(T-T_N)^{-3/2}$.

IV. SOUND VELOCITY

Following the procedure in the previous paper[5] we obtain from Eq. (3.3) the sound-frequency shift

$$\Delta\omega_{\vec{k}} = -(\beta/2\rho V\omega_{\vec{k}}^0)\langle(U_{\vec{k},1}+U_{\vec{k},2})(U_{-\vec{k},1}+U_{-\vec{k},2})\rangle. \tag{4.1}$$

If we use Eq. (2.10) for $U_{\vec{k},1}$ and Eq. (2.11) for $U_{\vec{k},2}$, $\Delta\omega_{\vec{k}}$ is expressed as a function of four-spin correlations. In the same way as the attenuation case, the four-spin correlation function is decoupled into a product of the two-spin correlation functions, and these two-spin correlation functions are replaced by the staggered susceptibilities, using the relation (3.9). Then, the velocity change is calculated as

$$\Delta v_t = \Delta\omega_{\vec{k}}/k = -[\rho V v_t(g\mu_B)^4k^2]^{-1}\Big(2|g_0^x(\vec{k})|^2(g\mu_B\langle S_0^x\rangle)^2\chi_{\vec{q}}^x + k_BT\sum_{\vec{q}}|g_{\vec{q}}^x(\vec{k})|^2(\chi_{\vec{q}}^x)^2 + k_BT\sum_{\vec{q}}|g_{\vec{q}}^y(\vec{k})|^2(\chi_{\vec{q}}^x)^2 + k_BT\sum_{\vec{q}}|g_{\vec{q}}^z(\vec{k})+h(\vec{k})|^2(\chi_{\vec{q}}^z)^2\Big). \tag{4.2}$$

Inserting Eq. (3.12) into Eq. (4.2) and making the summation of $\vec{q}$ in Eq. (4.2) over the Brillouin zone, we have

$$\Delta v_t = -F_{\vec{k}}'\Big[2\sigma_x^2\Big(\frac{G_x}{1-2J_0G_x}\Big) + \frac{k_BTv_0}{16\pi D}\Big(\frac{G_x}{1-2J_0G_x}\Big)^{1/2}\Big/(\omega_x^{1/2}-D_{\parallel})^{1/2} + \frac{k_BTv_0}{16\pi D}\Big(\frac{G_y}{1-2J_0G_y}\Big)^{1/2}\Big/(\omega_y^{1/2}-D_{\parallel})^{1/2}$$
$$+ \frac{k_BTv_0}{16\pi D}\frac{|g_0^z(\vec{k})+h(\vec{k})|^2}{|g_0^x(\vec{k})|^2}\Big(\frac{G_z}{1-2J_0G_z}\Big)^{1/2}\Big/(\omega_z^{1/2}-D_{\parallel})^{1/2}\Big], \tag{4.3}$$

$$F_{\vec{k}}'' = \frac{N|g_0^x(\vec{k})|^2}{\rho V v_t k^2}. \tag{4.4}$$

In the paramagnetic phase and in the absence of a magnetic field, Eq. (4.3) reduces to the usual mean-field-theory result which gives ΔV_l proportional to $(T - T_N)^{-1/2}$.

V. EXPERIMENT

A. Procedure

We obtained our data on a sample of single-crystal terbium obtained from Metals Research, Ltd. The sample was cylindrical in shape, having a diameter and length of 0.61 cm and 1.36 cm, respectively. The ends of the sample were cut normal to the c axis of the hcp crystallographic structure. A 15-MHz fundamental x-cut (longitudinal wave) quartz transducer was bonded to one end of the sample using an epoxy bonding process.[28] Figure 1 shows the experimental arrangement.

The pulse-echo technique was employed in monitoring the ultrasonic attenuation with a commercially available Matec package. Except where specifically noted, the data presented in this paper are double-echo type. We anticipated that sample deformations might occur when the temperature and applied magnetic field were changed, which could alter the bond coupling the transducer to the sample. The double-echo method of signal analysis virtually eliminates such nonintrinsic effects from the data.

The temperature was monitored via a copper-constantan thermocouple and controlled by a thermocouple feedback-energized heater system. The absolute accuracy of the temperature data is estimated to be ±0.5 °K, while the relative accuracy is estimated as ±0.1 °K.

Signal frequencies were measured by visually displaying and superposing the Matec pulse and a continuous wave of known frequency on the screen of a model 7904 Tektronix oscilloscope. The frequency range employed was 15–225 MHz.

The sample was suspended in a controlled environment provided by a standard ^{4}He cryogenic system. Highly uniform magnetic fields were supplied by a 15-in. Varian electromagnet, producing fields up to 17 kOe with a field inhomogeneity of seven parts in 10^5 over a cube with $\frac{1}{2}$-in. sides. The field was applied normal to the c axis of the crystal.

B. Results

In Fig. 2 we show the 15-MHz longitudinal ultrasonic attenuation in terbium from room temperature to 50 °K. The significant feature is the rather large attenuation peak at 219.7 °K with an accompanying shoulder around 225 °K, which we associate with the two magnetic-ordering phase transitions in terbium: the paramagnetic to spin-spiral transition at the higher temperature, and the spin-spiral to ferromagnetic transition at the lower temperature. For these data the external magnetic field (H) is zero, and the behavior agrees qualitatively with previously reported data.[1-3,29] In Fig. 3 we have plotted the attenuation as a function of temperature in the paramagnetic region for several frequencies in the range 15–225 MHz with $H = 0$. For each frequency the zero of attenuation was found by raising the temperature to about 300 °K where the attenuation is relatively unaffected by temperature changes, and using this high-temperature attenuation level as the reference level. In Fig. 4, we show the frequency dependence of the data in Fig. 3 at five representative temperatures. The attenuation is plotted against the square of the ultrasonic frequency, giving a fairly good linear fit and indicating a quadratic dependence of the atten-

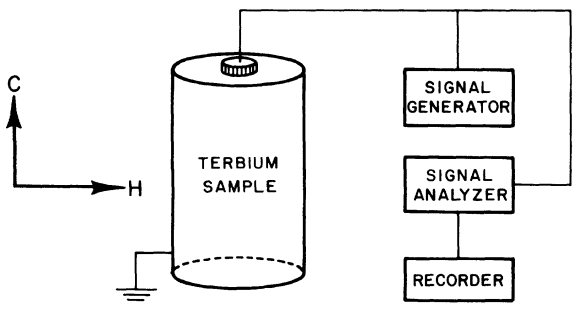

FIG. 1. Diagram illustrating the experimental arrangement. The transducer, depicted at the cylinder end, acts as both signal transmitter and receiver. The c axis coincides with the cylinder axis; H is normal to the c axis.

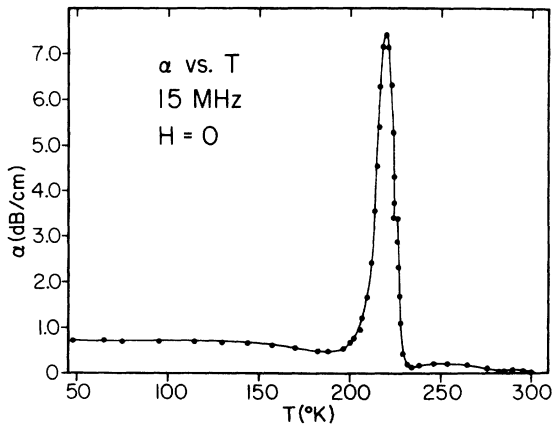

FIG. 2. Zero-field attenuation of 15-MHz longitudinal sound waves propagating along the c axis in single-crystal terbium.

uation on the impressed frequency. The theory which we have proposed in explanation of our attenuation data gives a quadratic frequency dependence for the attenuation, in agreement with our data. This quadratic frequency dependence of the attenuation in Tb was previously observed by Pollina and Luthi.[1] Also, this frequency dependence is typical of zero-field attenuation theories.

The rest of the data to be presented here are a study of the behavior of the ultrasonic attenuation for nonzero applied magnetic field. For completeness, two types of data will be given: that for which the frequency and temperature were constant while the magnetic field was slowly increased at a rate of about 2 kOe/min, and that for which the frequency and magnetic field were constant while the temperature slowly decreased at a rate of about 0.5 °K/min. The following data were obtained at the impressed frequency of 15 MHz only. This is purely an experimental simplification to ensure that good double-echo data could be obtained; the next-highest accessible frequency was 45 MHz, but the quadratic dependence on frequency plus the length of our sample made the attenuation so large that the second echo was often undetectable in the critical region. It was therefore advantageous to work at the lowest possible frequency, the fundamental transducer frequency of 15 MHz.

Figure 5 shows the attenuation plotted against the applied magnetic field H for several temperatures. The low-field region exhibits very large attenuation enhancement; we ascribe this enhancement to the spin polarization induced by the external field. Since the attenuation depends on the product of the spin polarization and a fluctuation-dependent term, the attenuation

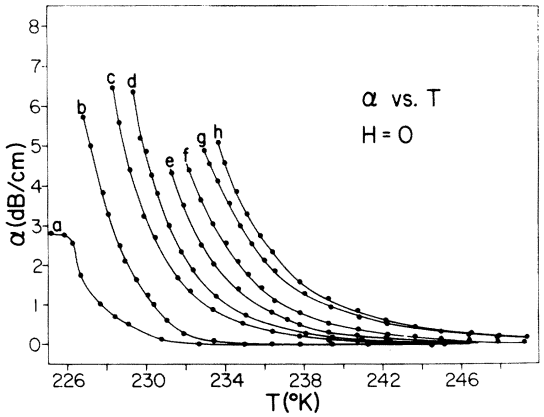

FIG. 3. Zero-field attenuation vs temperature data at the following measured frequencies (MHz): (a) 15.0, (b) 46.8, (c) 76.6, (d) 106.4, (e) 137.4, (f) 166.2, (g) 200.8, (h) 227.5.

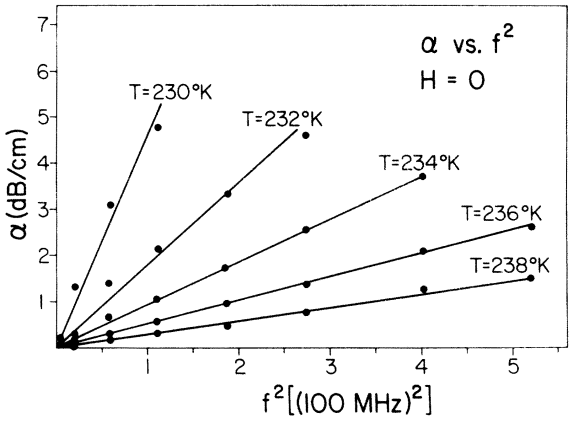

FIG. 4. Attenuation data from Fig. 3 plotted against the square of the sound wave frequency at five representative temperatures in the paramagnetic region.

reaches a maximum and thereafter decreases in magnitude as the magnetic field increases. A theoretical fit to the data in Fig. 5 will be discussed in Sec. VI (Fig. 11).

The data from Fig. 5 are replotted in Fig. 6 for the low-field region as a function of the square of the magnetic field. Since the graphs are linear, we conclude that the attenuation is quadratic in H for small H, in the paramagnetic region. This is to be expected, on the basis of our theoretical model, since the attenuation depends on the square of the induced spin polarization, which in turn ought to be linear in H

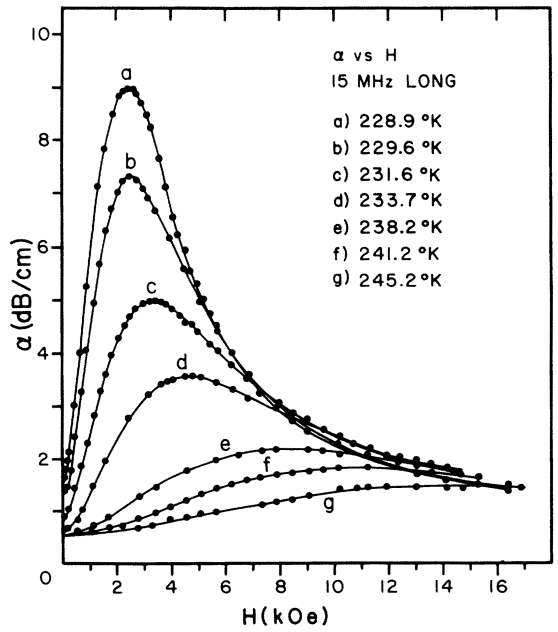

FIG. 5. Constant-temperature data for attentuation as a function of applied field.

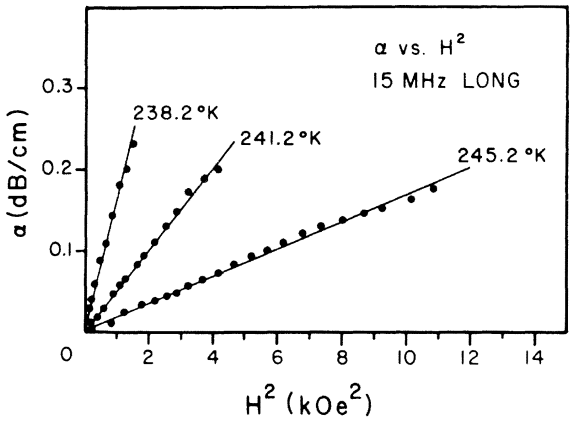

FIG. 6. Low-field region from Fig. 5, showing quadratic behavior of attenuation for small H.

for small H. Similar results have been reported for holmium[30] and MnP.[5,6]

In Fig. 7 we have plotted the attenuation as a function of temperature as the sample was cooled through the critical region in a constant small magnetic field. Of particular interest is the magnitude of the enhancement which results eventually in a second peak aroung $H = 1$ kOe. This enhancement continues as H is increased to 2.5 kOe, as shown in Fig. 8. Further increase of the applied field reduces the attenuation, as shown in Fig. 9. Qualitative agreement of our theoretical attenuation expression with the data in Fig. 9 will be shown in Fig. 12.

In Figs. 8 and 9 it was necessary to use both single- and double-echo techniques to obtain the data shown, due to the large total attenuation in our sample. For magnetic fields $2 \leq H \leq 3.5$ kOe we found that the second echo was near or

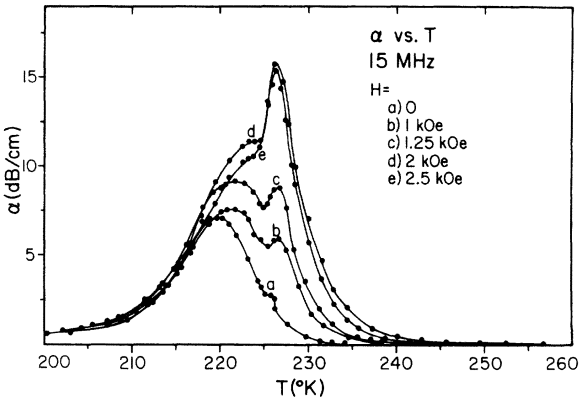

FIG. 8. Constant-field attenuation data showing maximum enhancement.

in the noise level when the temperature was at the point of maximum attenuation. We therefore made duplicate runs using the single- and double-echo methods and matched the two types of data at temperatures above and below the transition temperature to get complete information about the entire temperature region of interest.

An obvious feature of the attenuation versus temperature data, besides the aforementioned enhancement, is the shift in temperature of the attenuation maxima when the applied field changes. By associating these maxima with magnetic phase transitions, one can get a picture of the magnetic phase diagram implied by the data. The particular shape taken by the attenuation versus temperature curves is assumed to arise from the relatively close proximity of the transition temperatures T_N and T_C.

By picking up the attenuation-maxima temperatures and plotting them against the corre-

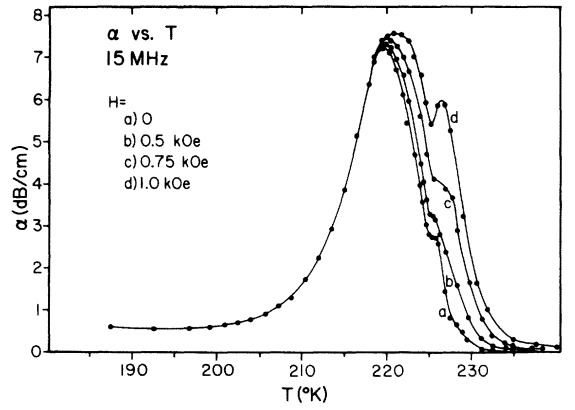

FIG. 7. Constant-field attenuation data when H is small. Note enhancement which leads to another maximum.

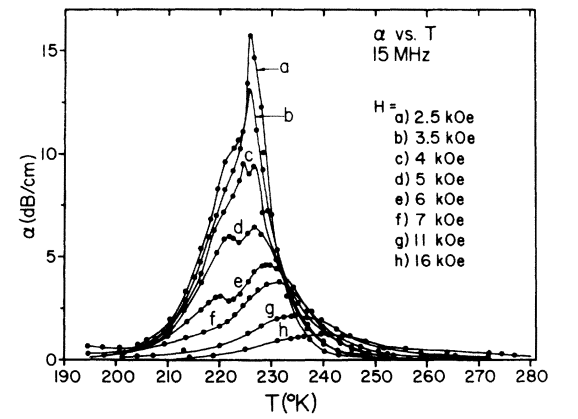

FIG. 9. Constant-field attenuation data showing onset of suppression produced by the applied field.

sponding magnetic field strengths, one gets the graph shown in Fig. 10. This graph can be viewed as an approximation to the magnetic phase diagram of terbium and interpreted as follows: the curves emanating from the $H=0$ axis mark the Néel and Curie temperatures, T_N and T_C; the application of a magnetic field moves T_N and T_C toward each other, until the critical field $H_c=3.5$ kOe is reached and T_N coincides with T_C; for fields higher than H_c one expects a uniform phase, varying continuously from a more paramagneticlike phase in the high-temperature region to the more ferromagnetic type as the temperature is decreased. The paramagnetic region is labeled A and the spin-spiral region is labeled B. Regions A, F-I, and F-II, for fields greater than H_c, are considered to be different regions of the uniform phase, where region F-I is more ferrolike than A, and region F-II is more ferrolike than F-I. The existence of attenuation maxima in the uniform-phase region may be attributable to fluctuations due to the onset of short-range ordering parallel to and perpendicular to the applied field in the basal plane; short-range ordering parallel to H (ferrolike) would be expected to occur at a higher temperature than short-range ordering perpendicular to H.

An important point to note here is that in Fig. 10 we used the external magnetic field, not the internal effective field, as the field responsible for the phase transitions. Because of the cylindrical shape of our sample, one must consider the contribution of the demagnetizing fields to the local magnetic field seen by the spins. The ratio of the length to the diameter in our sample is 2.24.

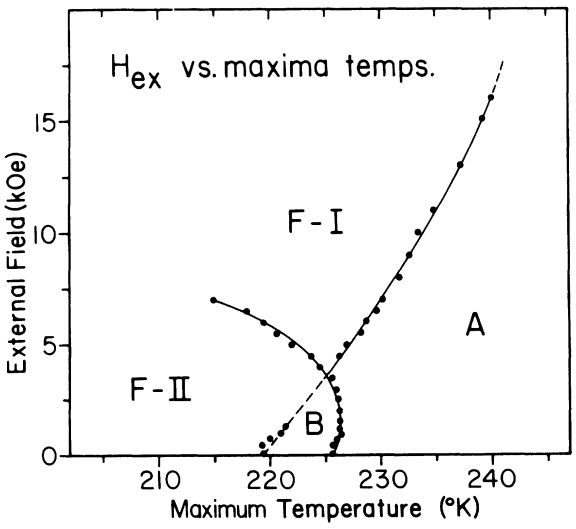

FIG. 10. Graph of the constant-field attenuation maxima showing the applied fields and corresponding temperatures at which they occur.

Using the table by Bozorth,[31] the demagnetizing factor along the cylinder axis is about $0.12(4\pi)$. The table lists demagnetizing factors when the external field is along the cylinder axis. However, our experiments were done with the external field normal to the cylinder axis. For cylinders, we have approximately

$$N_{\parallel}+2N_{\perp}=4\pi$$

in cgs units, whence

$$N_{\perp}=\tfrac{1}{2}(4\pi-N_{\parallel})=\tfrac{1}{2}[4\pi-0.12(4\pi)]=5.53.$$

Using the magnetization data of Hegland *et al.*[32] for Tb for a reduced temperature of $T/T_N=225/226.3=0.994$, we may compute

$$H_i+N_{\perp}M=H_{\text{ext}},$$

where H_i is the internal field. In this way one finds that $H_{ex}\approx 3.5$ kOe for $H_i\approx 820$ Oe. Therefore our experimentally determined value of the critical field, $H_c\approx 3.5$ kOe (Fig. 10), at $T/T_N=0.994$ implies an internal-field strength of about 820 Oe; this is in good agreement with the data of Thoburn *et al.*[33] and Hegland *et al.*,[32] their value being 800 Oe for the field sufficient to quench the spin-spiral state.

VI. EXPLANATION OF EXPERIMENTAL RESULTS

A. Attenuation of longitudinal sound

The parameters which are contained in the expression of the attenuation coefficient, Eq. (3.14), are determined in the following way. The anisotropy constant D is related to the parallel paramagnetic Curie temperature $\theta_{\parallel}$ and the perpendicular paramagnetic Curie temperature $\theta_{\perp}$ with the relation

$$k_B(\theta_{\perp}-\theta_{\parallel})=\tfrac{1}{10}D[4S(S+1)-3]. \qquad (6.1)$$

By using the value of $\theta_{\perp}-\theta_{\parallel}=44\,^{\circ}\text{K}$,[32] D is determined to be $D=1.57\,^{\circ}\text{K}$. Jenson[2] has obtained the elastic constant c^{γ} on Tb by measuring the shear-elastic-wave velocity at room temperature. He finds $c^{\gamma}=9.20\times 10^{11}$ dyn/cm^2. The magnetostriction coefficient λ^{γ} has been determined by Rhyne and Legvold[21] to be $\lambda^{\gamma}(T=0)=8.8\times 10^{-3}$. Using this value and the relation $\tilde{B}^{\gamma}=2c^{\gamma}\lambda^{\gamma}/S(2S-1)$, we estimate $\tilde{B}^{\gamma}$ as 50 °K/atom. Marsh and Sievers,[34] Wagner and Stanford,[15] and Sievers[35] have made magnetic-resonance experiments and estimated the value of $\tilde{B}^{\gamma}$ from the gap of the spin-wave and the anisotropy constants on the basis of the frozen-

lattice model to be 76 °K/atom (Marsh and Sievers), 64.4 °K/atom (Wagner and Stanford), and 100 °K/atom (Sievers). We tentatively take 100 °K/atom for $\tilde{B}^{\gamma}$.

The parameters J_0, $D_{\parallel}$, and A in Eq. (3.12) are related to Q, T_N, and H_c: (i) The wave number Q which is a function of $D_{\parallel}$ and A, as seen in Eq. (3.13), ranges from $0.115(2\pi/c_0)$ to $0.095(2\pi/c_0)$ depending on the temperature.[27] We take $0.10(2\pi/c_0)$ for Q and neglect the temperature dependence of Q. (ii) In the mean-field approximation, the Néel temperature is expressed as

$$k_B T_N = \frac{S(S+1)}{3}\left(2J_0 + \frac{D_{\parallel}^2}{4A}\right)\left(1 + \frac{D}{30k_B T_N}[4S(S+1) - 3]\right). \tag{6.2}$$

In general, this equation gives a transition temperature which is higher than the real value, since this equation does not include the contribution of the spin fluctuation to the energy. Therefore, T_N should rather be considered as a parameter which may be adjusted to find the best agreement with the experimental data. We take 228.5 for T_N. From these expressions for Q and T_N, J_0 and $D_{\parallel}$ are expressed as functions of A. (iii) The paramagnetic to spin spiral transition is of second order and $\chi_{\vec{Q}}^{\gamma}$ diverges at this transition point. When A is fixed, T_N decreases with increasing magnetic field, and above a certain value of the magnetic field $\chi_{\vec{Q}}^{\gamma}$ does not diverge at any temperature, since the spin-spiral phase disappears above the critical field H_c. The value of H_c is a function of the parameter A, and H_c coincides with our experimental value of 3.5 kOe for $A = 1.624c_0^4$ °K. In order to facilitate comparison with the experimental data the effect of the demagnetization factor has been absorbed into this value of A by using $H_c = 3.5$ kOe instead of $H_c = 820$ Oe. From the values of A, T_N, and Q, J_0, and $D_{\parallel}$ are determined to be 7.717 °K and $1.297c_1^2$ °K, respectively. We leave $D_{\perp}$ in Eq. (3.12) as an adjustable parameter and determine it by comparison with the field dependence of the attenuation coefficient.

First we calculate the attenuation coefficient when the temperature is fixed and the magnetic field is changed. The expression of the attenuation coefficient is given by Eq. (3.14). If $|h(\vec{k})|$ is comparable to $|g_0^z(\vec{k})|$, the last term in the square bracket of Eq. (3.14) is negligibly small compared with the other terms in the vicinity of the critical temperature, since the spin fluctuation along the c axis is strongly suppressed. For determining the adjustable parameter $D_{\perp}/v_0$, we calculated $\alpha_{\vec{k}}^{\vec{\tau}}/F_{\vec{k}}^{\vec{\tau}}$ as a function of the magnetic field and the parameter $D_{\perp}/v_0$, holding the temperature at 233.7 °K. The calculated $\alpha_{\vec{k}}^{\vec{\tau}}/F_{\vec{k}}^{\vec{\tau}}$ has a maximum at a certain magnetic field whose value depends on the magnitude of $D_{\perp}/v_0$ and which coincides with the experimental value of 5 kOe when $D_{\perp}/v_0$ is 90 °K/c_0. The value of $F_{\vec{k}}^{\vec{\tau}}$ is determined from the magnitude of the attenuation at the maximum point. Using these values, we obtain the field dependence of the attenuation coefficient for various temperatures and show the results in Fig. 11. As seen from the figure, agreement between theory and experiment is satisfactory. We did not show the calculated values of the attenuation corresponding to 228.9 and 229.6 °K in the figure for the following reason: The attenuation coefficient is expressed as a function of susceptibilities, as seen in Eq. (3.11); but the susceptibility calculated by the mean-field approximation does not agree with experimental observations at temperatures within $\frac{1}{2}\%$ of the zero-field Néel temperature. Therefore it would not be expected that the theoretical curve for $\alpha_{\vec{k}}^{\vec{\tau}}$ would agree with the experimental data within this temperature range.

Figure 12 shows the temperature dependence of the attenuation coefficient for several values of magnetic field above H_c. Curve a, which corre-

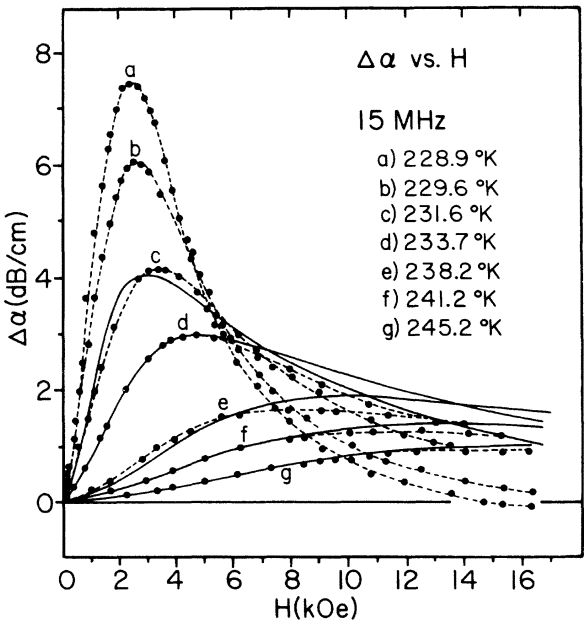

FIG. 11. Magnetic field dependence of the attenuation in Tb measured from that in zero-field: $\Delta\alpha_K(H) = \alpha_K(H) - \alpha_K(0)$. Solid lines represent the calculated values using Eq. (3.14), and black dots show the experimental values.

sponds to a magnetic field just above H_c, has a large maximum at a low temperature and a shoulder at a high temperature. The low-temperature peak decreases rapidly with increasing field. The characteristics exhibited here are seen in the experimental curves of Fig. 9.

The attenuation peak at the lower temperature comes from the contribution of the y-component term in the large parentheses in Eq. (3.11). This peak may be understood as follows. The exchange interaction acts on spins to order them with the wave number $\vec{Q}$, and thus enhances χ^y_Q. At high temperatures, this effect is weakened by the thermal agitation of spins and χ^y_Q decreases. On the other hand, at low temperatures the magnetoelastic interaction suppresses the spin fluctuations in the y direction, and thus this interaction decreases χ^y_Q. As a result, χ^y_Q has a maximum at an intermediate temperature near T_N. This maximum leads to the maximum of the attenuation coefficient at the lower temperature. The attenuation peak at the higher temperature comes mainly from the first term in the large parentheses in Eq. (3.11). In a magnetic field the magnitude of the product of $\langle S^x_0 \rangle$ and χ^x_k has a maximum slightly above T_N. Therefore we have two peaks in the attenuation coefficient above H_c. The low-temperature peak is just a function of χ^y_Q. The susceptibility and thus the peak height rapidly decrease with increasing magnetic field. This is apparent by the rapid decrease and eventual disappearance of the low-temperature peak both experimentally (Fig. 9) and theoretically (Fig. 12) as the magnetic field is increased. On the other hand, the high-temperature peak is proportional to the square of the product of $\langle S^x_0 \rangle$ and χ^x_k. Since $\langle S^x_0 \rangle$ is an increasing quantity with magnetic field, the decreasing rate of the product $\langle S^x_0 \rangle \chi^x_k$ in a magnetic field is weakened compared with that of χ^x_k. Consequently, the decreasing rate of the high-temperature peak is much smaller than that of the low-temperature peak as seen in Figs. 9 and 12. The phase diagram obtained in our experiment (Fig. 10) shows the change of the short-range order of the spins as well as that of the long-range order. When the temperature decreases in a magnetic field above H_c, the short-range order of the spin component in the field direction becomes maximal at the boundary between the A and F-I phases. With further decreasing temperatures, the sinusoidal short-range order of the spin component perpendicular to the field direction in the c plane becomes maximal around the boundary between the F-I and F-II phases.

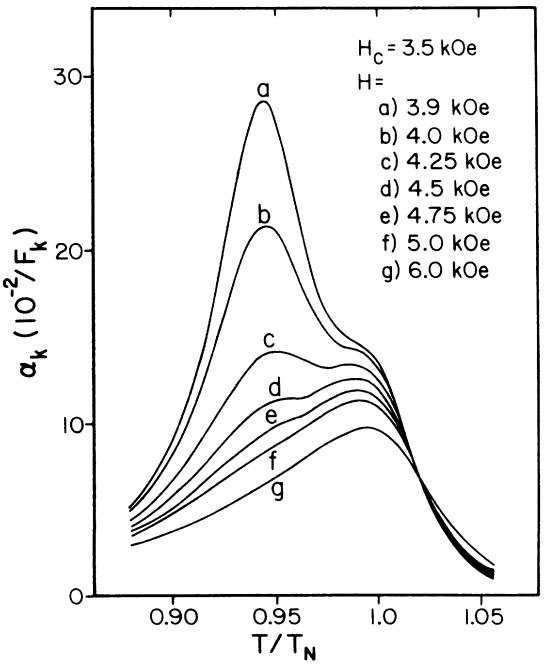

FIG. 12. Temperature dependence of the attenuation in a magnetic field applied normal to the c axis, calculated from Eq. (3.14). This behavior is to be compared to the experimental data in Fig. 9.

B. Velocity change of longitudinal sound

Lüthi *et al.*[4] have measured the sound velocity change of Gd, Tb, Ho, and Dy in a magnetic field. They plotted the relative change for a 10 kOe field $\Delta v_l = [v_l(H,T) - v_l(0,T)]/v_l(0,T)$ vs $T - T_N$, where $v_l(H,T)$ is the velocity in a field H at a temperature T. Their results for Gd, Tb, and Ho, are as follows: Δv_l is negative for most of the paramagnetic phase and is positive only close to T_N ($T - T_N \leq 0.1 T_N$). Below T_N, Δv_l is positive. We calculated Δv_l at fields of 5, 10, and 15 kOe in the paramagnetic region using Eq. (4.3). The last term in Eq. (4.3), which originates from spin fluctuations in the z direction, can be neglected owing to the large uniaxial anisotropy as discussed in the case of the attenuation. The parameter F^t_k/v_l was determined from the experimental value at a 10 kOe field and a temperature of $T - T_N = 5$ °K. The temperature dependence of Δv_l is shown in Fig. 13. This temperature variation is in agreement with the experimental results mentioned above. The drastic temperature variation of Δv_l is due to the following facts. The magnitude of the dip in the velocity change at T_N diverges in the absence of a magnetic field. However, in a magnetic field this diverges disappears. This effect makes Δv_l positive very close to T_N. The fact that Δv_l is negative for most of the paramagnetic phase is

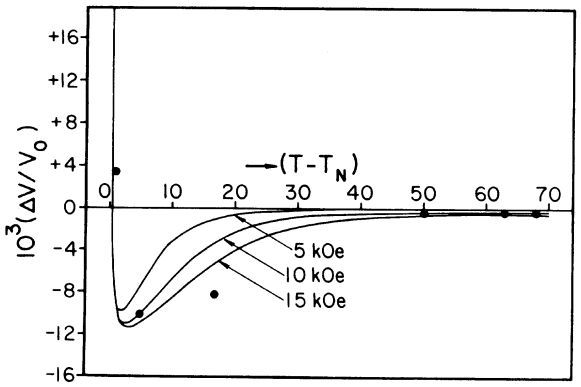

FIG. 13. Calculated values of ultrasonic velocity change using Eq. (4.3). Black dots are experimental data points obtained by Lüthi *et al.* (Ref. 4) for Tb.

due to the large positive magnetic field dependence of the first term in the large parentheses in Eq. (4.2). As may be seen the principal magnetic field dependence of this term comes from $\langle S_0^z \rangle^2$.

VII. CONCLUDING REMARKS

We studied longitudinal sound propagation in Tb under a magnetic field, with emphasis on the contribution of spin fluctuations on the sound attenuation. In this respect the following properties of Tb were significant: First, the exchange energies between the ferromagnetic and the spin-spiral states are very close–therefore, when we consider the critical fluctuations of spins we must treat both the ferromagnetic and sinusoidal spin fluctuations at the same time; second, the magnetoelastic interaction has a significant effect on the spin fluctuations.

We have observed strong enhancement of the attenuation by the magnetic field in the paramagnetic phase near T_N. The model we have proposed has explained this enhancement and the complicated velocity change in a magnetic field observed by Lüthi *et al.*[4]

We obtained the phase diagram of Tb which shows the change of the short-range order of spins as well as that of the long-range order. We estimated the critical value of the internal field, at which the spin-spiral phase disappears, as 820 Oe.

In addition to the two peaks which originate from the phase transitions, we have observed two anomalous peaks by increasing the external field beyond the critical field. We explained these two anomalous peaks as follows: The spin fluctuations become anisotropic in the magnetic field. When we change temperature with a fixed value of the field, the properties of the spin fluctuations do not change monotonically but change rapidly around a certain temperature in a uniform phase. This rapid change occurs in each component of spin almost independently, and leads to the anomalous attenuation peak. The magnetic field leads to a maximum of the spin fluctuation in the field direction and the magnetostriction leads to a maximum of the spin fluctuation perpendicular to the field direction. Thus it appears that ultrasonic attenuation is very useful not only for studying phase transitions of magnetic systems but also for studying changes in the short-range order of spins as a function of temperature and magnetic field.

ACKNOWLEDGMENTS

The authors wish to express their gratitude to I-An Feng and Harry Salvo for their assistance in this work.

APPENDIX

When we define a and A_n as

$$a=-\beta(-2\tilde{J}_0\sigma_x+g\mu_B H), \tag{A1}$$

and

$$A_n=\sum_{m=-s}^{s} m^n e^{am}, \tag{A2}$$

we have

$$\beta^{-1}G_x=\left(\frac{A_2}{A_0}\right)-\left(\frac{A_1}{A_0}\right)^2+\frac{\beta D}{2}\left[\left(\frac{A_4}{A_0}\right)-3\left(\frac{A_1A_3}{A_0^2}\right)+2\left(\frac{A_1^2A_2}{A_0^3}\right)-\left(\frac{A_2}{A_0}\right)^2\right]-\frac{3\beta(\tilde{B}^\gamma)^2}{16c^\gamma}\left[S(S+1)-3\left(\frac{A_2}{A_0}\right)\right]$$

$$\times\left[\left(\frac{A_4}{A_0}\right)-3\left(\frac{A_1A_3}{A_0^3}\right)+2\left(\frac{A_1^2A_2}{A_0^3}\right)-\left(\frac{A_2}{A_0}\right)^2\right]+\frac{9\beta(\tilde{B}^\gamma)^2}{16c^\gamma}\left[\left(\frac{A_3}{A_0}\right)-\left(\frac{A_1A_2}{A_0^2}\right)\right]^2, \tag{A3}$$

$$\beta^{-1}G_y=\frac{Yc}{2A_0a}-\frac{D}{4aA_0}\left(\frac{Y_d}{2a}+\frac{Y_cA_2}{A_0}-Y_cS(S+1)\right)$$

$$-\frac{\beta(\tilde{B}^\gamma)^2}{8c^\gamma aA_0}\left[S(S+1)-3\left(\frac{A_2}{A_0}\right)\right]\left[\frac{Y_d}{8a}+\frac{Y_b}{a}-\frac{3Y_cA_2}{4A_0}-\frac{Y_c}{4}S(S+1)\right], \tag{A4}$$

$$Y_c=-(\sinh a)A_2-2(\sinh\tfrac{1}{2}a)^2A_1+S(S+1)(\sinh a)A_0, \tag{A5}$$

$$Y_b = A_0 S(S+1)(1 + a\sinh a - \cosh a) + A_1[2S(S+1) - 1](a\cosh a - \sinh a)$$
$$+ A_2[S(S+1)a\sinh a - 3a\sinh a - 3 + 3\cosh a]$$
$$- A_3(3a\cosh a - 2\sinh a - a) - A_4 a\sinh a, \tag{A6}$$

$$Y_d = A_0[S^2(S+1)^2(\tfrac{1}{2} - \tfrac{1}{2}\cosh 2a + 2a\sinh a) + S(S+1)(-1 + \cosh 2a - 2a\sinh a)]$$
$$+ A_1[2S(S+1)(a + \sinh 2a - 3a\cosh a) + 2a\cosh a - \sinh 2a]$$
$$+ A_2[S(S+1)(\cosh 2a - 4a\sinh a - 1) + \tfrac{5}{2} + \tfrac{5}{2}\cosh 2a + 6a\sinh a]$$
$$+ 2A_3(2a\cosh a - \sinh 2a - a) + A_4(2a\sinh a - \tfrac{1}{2}\cosh 2a + \tfrac{1}{2}), \tag{A7}$$

$$\beta^{-1}G_z = \frac{Z_c}{A_0} - \frac{\beta D}{A_0}\left[Z_d - \tfrac{1}{2}S(S+1)Z_c + \frac{A_2 Z_c}{2A_0}\right] - \frac{\beta(\tilde{B}^\gamma)^2}{4c^\gamma A_0}\left[S(S+1) - 3\left(\frac{A_2}{A_0}\right)\right]\left[\frac{Z_d}{2} + Z_b - \frac{3A_2 Z_c}{4A_0} - \frac{S(S+1)Z_c}{4}\right], \tag{A8}$$

$$Z_c = \frac{A_0}{2a}\left[(\sinh a)S(S+1) + (1 - \cosh a)\left(\frac{A_1}{A_0}\right) - (\sinh a)\left(\frac{A_2}{A_0}\right)\right], \tag{A9}$$

$$Z_b = \frac{A_0}{2a^2}\left\{S(S+1)\left[1 + a\sinh a - \cosh a - 2\left(\frac{A_1}{A_0}\right)(\sinh a - a\cosh a) + a\sinh a\left(\frac{A_2}{A_0}\right)\right]\right.$$
$$+ (\sinh a - a\cosh a)\left(\frac{A_1}{A_0}\right) - 3(1 + a\sinh a - \cosh a)\left(\frac{A_2}{A_0}\right)$$
$$\left. + (a + 2\sinh a - 3a\cosh a)\left(\frac{A_3}{A_0}\right) - a\sinh a\left(\frac{A_4}{A_0}\right)\right\}, \tag{A10}$$

$$Z_d = -\frac{A_0}{8a^2}\left\{(1 - \cosh a)\left[S^2(S+1)^2 - [2S(S+1)+1]\left(\frac{A_2}{A_0}\right) + \left(\frac{A_4}{A_0}\right)\right]\right.$$
$$- 2(1 + a\sinh a - \cosh a)\left[S^2(S+1)^2 - S(S+1) - 2S(S+1)\left(\frac{A_2}{A_0}\right) + 3\left(\frac{A_2}{A_0}\right) + \left(\frac{A_4}{A_0}\right)\right]$$
$$+ 2(\sinh a - a\cosh a)\left[-3S(S+1)\left(\frac{A_1}{A_0}\right) + \left(\frac{A_1}{A_0}\right) + 3\left(\frac{A_3}{A_0}\right)\right]$$
$$+ 2(1 - \cosh a)\left[S^2(S+1)^2 - 2S(S+1)\left(\frac{A_2}{A_0}\right) + \left(\frac{A_4}{A_0}\right)\right] + 2(a - \sinh a)\left[-S(S+1)\left(\frac{A_1}{A_0}\right) + \left(\frac{A_3}{A_0}\right)\right]$$
$$- \tfrac{1}{2}(1 + \cosh 2a - 2\cosh a)\left[S^2(S+1)^2 - 2S(S+1) - 2S(S+1)\left(\frac{A_2}{A_0}\right) + 5\left(\frac{A_2}{A_0}\right) + \left(\frac{A_4}{A_0}\right)\right]$$
$$\left. + \tfrac{1}{2}(2\sinh a - \sinh 2a)\left[-4S(S+1)\left(\frac{A_1}{A_0}\right) + 2\left(\frac{A_1}{A_0}\right) + 4\left(\frac{A_3}{A_0}\right)\right]\right\}. \tag{A11}$$

When the spin polarization σ_z is less than 0.3 times the spin value S, G_μ is expressed as

$$\beta^{-1}G_x = \frac{S(S+1)}{3}\left[1 - \frac{a^2}{10}[S^2 + (S+1)^2]\right] + \frac{\beta D}{90}S(S+1)[4S(S+1) - 3] + \frac{\beta(\tilde{B}^\gamma)^2}{2400c^\gamma}S^2(S+1)^2[4S(S+1) - 3]^2 a^2, \tag{A12}$$

$$\beta^{-1}G_y = \frac{S(S+1)}{3}\left[1 - \frac{a^2}{30}[S^2 + (S+1)^2]\right] + \frac{\beta D}{90}S(S+1)[4S(S+1) - 3] - \frac{\beta(\tilde{B}^\gamma)^2}{240c^\gamma}S^2(S+1)^2[4S(S+1) - 3]^2 a^2, \tag{A13}$$

$$\beta^{-1}G_z = \frac{S(S+1)}{3}\left[1 - \frac{a^2}{30}[S^2 + (S+1)^2]\right] - \frac{\beta D}{45}S(S+1)[4S(S+1) - 3]. \tag{A14}$$

*Research supported by the U. S. Air Force Office of Scientific Research under Grant No. AFOSR 71-2079.

†Temporary address: IBM Thomas J. Watson Research Center, Yorktown Heights, N. Y. 10598.

‡Permanent address: Tohoku University, Sendai, Japan.

§Permanent address: Wyle Laboratory, El Segundo, Calif. 90245.

[1]R. J. Pollina and B. Luthi, Phys. Rev. 177, 841 (1969).

[2]J. Jenson, Riso Report No. 252, Danish Atomic Energy Commission, DK-4000, Roshilde, Denmark (1971) (unpublished).

[3]M. Rosen, Phys. Rev. 174, 504 (1968).

[4]B. Lüthi, T. J. Moran, and R. J. Pollina, J. Phys. Chem. Solids 31, 1741 (1970).

[5]M. Tachiki and S. Maekawa, Prog. Theor. Phys. 51, 1 (1974).

[6]T. Komatsubara, A. Ishizaki, S. Kusaka, and E. Hirahara, Solid State Commun. 14, 741 (1974).

[7]B. Cooper, Phys. Rev. Lett. 19, 900 (1967).

[8]B. R. Cooper, in *Solid State Physics*, edited by F. Seitz, D. Turnbull, and H. Ehrenreich (Academic, New York, 1968), Vol. 21.

[9]B. Cooper, in *Magnetic Properties of Rare Earth Metals*, edited by R. J. Elliott (Plenum, New York, 1972).

[10]See, for example, T. Kasuya, in *Magnetism*, edited by G. T. Rado and H. Suhl (Academic, New York, 1966).

[11]J. J. Rhyne and A. E. Clark, J. Appl. Phys. 38, 1379 (1967).

[12]J. L. Stanford and R. C. Young, Phys. Rev. 157, 245 (1967).

[13]J. J. Rhyne, S. Foner, E. J. McNiff, and R. Doclo, J. Appl. Phys. 39, 892 (1968).

[14]R. Z. Levitin and B. K. Ponomarev, Zh. Eksp. Teor. Fiz. 53, 1978 (1967) [Sov. Phys.—JETP 26, 1121 (1968)].

[15]T. K. Wagner and J. L. Stanford, Phys. Rev. 184, 505 (1969).

[16]J. L. Feron, G. Huy, and R. Pauthenet, in *Les Elements des Terres Rares*, edited by A. H. Millhouse and W. C. Koehler (CNRS, Paris, 1970), Vol. II, p. 9.

[17]K. Tajima and S. Chikazumi, J. Phys. Soc. Jpn. 23, 1175 (1967).

[18]P. H. Bly, W. D. Corner, and K. N. R. Taylor, J. Appl. Phys. 39, 1336 (1968); 40, 4787 (1969).

[19]E. Callen and H. B. Callen, Phys. Rev. 138, A455 (1965).

[20]A. E. Clark, B. F. Desavage, and R. Borzorth, Phys. Rev. 138, A216 (1965).

[21]J. J. Rhyne and S. Legvold, Phys. Rev. 138, A507 (1965).

[22]D. B. McWhan, A. L. Stevens, Phys. Rev. 138, A682 (1965).

[23]A. Jayaraman, R. C. Sherwood, A. J. Williams, and E. Corezwitt, Phys. Rev. 148, 502 (1968).

[24]H. S. Bennett and E. Pytte, Phys. Rev. 155, 553 (1967); 164, 712 (1967); H. S. Bennett, *ibid.* 181, 978 (1969); K. Tani and H. Mori, Prog. Theor. Phys. 39, 876 (1968); H. Okamoto, *ibid.* 37, 1348 (1967); K. Kawasaki, Solid State Commun. 6, 57 (1968); Phys. Lett. A 26, 543 (1968); G. E. Laramore and L. P. Kadanoff, Phys. Rev. 187, 619 (1969).

[25]R. Kubo, J. Phys. Soc. Jpn. 12, 570 (1957).

[26]H. Mori, Prog. Theor. Phys. 33, 423 (1965).

[27]O. W. Dietrich and J. Als-Nielsen, J. Phys. C 4, 71 (1971).

[28]M. Levy and I. Rudnick, J. Acoust. Soc. Am. 34, 520 (1962).

[29]The word "qualitatively" is used because agreement on the shape of the curve exists, but the experiments were done at different frequencies and the maxima occur at different temperatures (probably due largely to varying impurity content).

[30]M. Tachiki, M. Lee, and M. Levy, Phys. Rev. Lett. 29, 488 (1972).

[31]R. Bozorth, in *Ferromagnetism* (Van Nostrand, Princeton, N. J., 1951).

[32]D. Hegland, S. Legvold, and F. H. Spedding, Phys. Rev. 131, 158 (1963).

[33]W. Thoburn, S. Legvold, and F. H. Spedding, Phys. Rev. 112, 56 (1968).

[34]H. S. Marsh and A. J. Sievers, J. Appl. Phys. 40, 1563 (1969).

[35]A. J. Sievers, J. Appl. Phys. 41, 980 (1970).